Journal of
Materials Chemistry A

N-boronated polybenzimidazole for composite electrolyte design of highly ion conductive pseudo solid-state ion gel electrolytes with high Li-transference number

Journal:	*Journal of Materials Chemistry A*
Manuscript ID	TA-ART-10-2018-010476.R1
Article Type:	Paper
Date Submitted by the Author:	19-Dec-2018
Complete List of Authors:	Nag, Aniruddha; Japan Advanced Institute of Science and Technology, Energy and environment Science; Ali, Mohammad Asif; Japan Advanced Institute of Sci. & Tech., Energy and Environment Area Singh, Ankit; Japan Advanced Institute of Science and Technology (JAIST), School of Materials Science Vedarajan, Raman; International Advanced Research Centre for Powder Metallurgy and New Materials, Centre for Fuel Cell Technology Matsumi, Noriyoshi; Japan Advanced Institute of Science and Technology (JAIST), School of Materials Science Kaneko, Tatsuo; Japan Advanced Institute of Science and Technology,

SCHOLARONE™
Manuscripts

Journal of Materials Chemistry A

ARTICLE

N-boronated polybenzimidazole for composite electrolyte design of highly ion conductive pseudo solid-state ion gel electrolytes with high Li-transference number

Aniruddha Nag[a], Mohammad Asif Ali[a], Ankit Singh[a], Raman Vedarajan[a, b], Noriyoshi Matsumi[a*], Tatsuo Kaneko[a*]

We prepared high ion conducting polymer electrolyte with high lithium transference number (t_{Li+}) using organoborane-modified polybenzimidazole (B-PBI) and ionic liquid (IL), 1-butyl-3-methylimidazolium bis(trifluoromethane-sulfonyl)imide (BMImTFSI). The structural characteristics of these electrolytes were examined by nuclear magnetic resonance and Fourier-transform infrared spectroscopy. Thermo-gravimetric analysis and dynamic viscosity measurements were used to investigate the thermal and rheological properties of the electrolytes. Unlike other solid polymer electrolyte systems, the addition of lithium salt was not required in the case of the electrolytes prepared in this study as the molecular designing already incorporates lithium. The amount of BMImTFSI (w/w %) affected the ion transport behaviour of the composite polymer electrolytes. The ionic conductivity of the electrolytes increased with an increase in the IL content. The electrolyte with B-PBI/BMImTFSI (w/w %) (25/75) showed the highest conductivity of 8.8×10^{-3} S cm^{-1} at 51 °C. It has also showed the highest t_{Li+} value of 0.63 at room temperature with wider electrochemical potential window of 5.45 V. The composite electrolytes were employed in anodic half-cells (Si/electrolyte/Li) and they showed high reversible capacity up to 1300 mAhg^{-1} and retained it even at high charging rate. Electrochemical impedance spectroscopy and dynamic electrochemical impedance spectroscopy were performed before and after the charge-discharge measurements to confirm the formation of stable solid electrolyte interface with B-PBI/BMImTFSI (w/w %).

Introduction

One of the recent advancements in the field of lithium-ion secondary batteries is the development of solid polymer electrolytes (SPEs), which can provide significantly higher energy density, longer cycle life and high safety as compared with liquid electrolyte based batteries[1-7]. Conventional solid polymer electrolytes (SPEs) such as poly(ethylene oxide) (PEO) suffer from very low lithium transference number because of the strong binding of their ether oxygen to lithium ions[8]. Two approaches have been used to increase the lithium transference number of these SPEs: 1) the covalent introduction of dissociable lithium salts (polymer salt hybrids)[9] or 2) the incorporation of anion receptors for selective Li-

ion transport[10-11]. In both approaches, boron chemistry[12-13] has been very useful in designing highly dissociable lithium salt structures and efficient anion receptors. Zhou *et al*. reported preparation of single lithium ion conducting polymer electrolyte by dissolving lithium salts in super-delocalized polyanions, and could attain high t_{Li+} with moderately high ionic conductivity[23-24]. Novel molecular design of solid-state electrolytes must induce better conductivity, which would enable high rate battery performance and also chemical and electrochemical compatibility with the electrode material[25]. The most promising approach to achieve high ionic conductivity along with satisfactory lithium transference number is to prepare polymer ion gel electrolytes using ionic liquids (ILs)[14]. Various types of polymer ion gel electrolytes have been reported thus far. However, only a few of these exhibited both high ionic conductivities and lithium transference numbers at the same time. Designing of solid polymer-salt hybrid electrolytes with highly dissociable lithium salt structures and their plasticization with ILs is expected to be a promising approach to prepare high performance pseudo solid electrolytes[15-17]. Furthermore, close observation and understanding of the potential profile across electrode/electrolyte interface is indispensible to check solid-state battery stability[18].

Due to structural advantages and thermo-mechanical stability polybenzmidazole group of polymers are well established in terms of energy applications as well as side-chain functionalization for several other possible applications[26-29]. In this study, we developed novel high-performance poly (2, 5-benzimidazole) type polymer electrolytes using 3, 4-diaminobenzoic acid (3, 4-DABA) as the starting material. The imidazole ring was modified to introduce lithium boroimidazolate to prepare SPE. An IL was added to the prepared SPEs while maintaining their solidity. The composition of the electrolytes was optimized to tailor ionic conductivity, potential window and t_{Li}^+ for the fabrication of anodic half-cells[19]. Dynamic electrochemical impedance spectroscopy (DEIS) was used for the real-time examination of the interfacial structure during the charging and discharging processes[20-22]. The composite polymer electrolytes showed maximum ionic conductivity of 8.8 x10^{-3} Scm^{-1} and maximum t_{Li}^+ of 0.63. They were carefully designed for application in secondary batteries. The Li/electrolyte/Si anodic half-cell showed a maximum discharging capacity of 1300 mAhg^{-1} at 0.1 C and could retain a capacity of 800 mAhg^{-1} even at the higher current rate of 2C with Coulombic efficiency of 92%.

Experimental section:

Synthesis of the homopolymer poly-(2, 5-benzimidazole) (ABPBI):

Poly (2, 5-benzimidazole) (ABPBI) was synthesized by the homo-polycondensation of 3, 4-diaminobenzoic acid (3, 4-DABA) (Scheme. 1). Poly(phosphoric acid) (PPA, $H_{n+2}P_nO_{3n+1}$) (13-15g. approx.) was purged with nitrogen gas in a 200 mL three-neck round-bottomed flask, which was maintained at 120 °C for 1 h to remove moisture completely. 3, 4-DABA.2HCl (0.58 g, 2.6 mmol) was then added to this flask and the mixture was maintained at 120 ℃ for 1 h. After homogenization, the temperature was increased to 180 °C and maintained for 2 h before increasing it further to 200°C, which was maintained for 3 h. The reaction mixture turned dark brown from yellow with time, and the viscosity of the mixture increased gradually with time. The resulting solution was precipitated over

water to obtain threads. These threads were then crushed, washed with water and dried at 100°C under vacuum. ABPBI powder was immersed in a 10% KOH solution overnight, and was then washed on a filter paper repeatedly with deionized water until the filtrate showed neutral *p*H. The resulting powder was then soaked in acetone and dried at 100 °C under vacuum for two days to finally obtain pure ABPBI polymer (yield 95%).

The structure of ABPBI was confirmed by Fourier transform infrared (FT-IR) spectroscopy (Figure 2(a)). The C=N peaks for imidazole groups were observed at around 1715 cm^{-1}. Aromatic C=C peaks were observed at 1650 cm^{-1} and broad –NH peaks were also clearly observed at 3300 cm^{-1}. The structure of ABPBI was further characterized by solid-state ^{13}C nuclear magnetic resonance (NMR (CP-TOSS) spectroscopy. Five broad ^{13}C signals appeared over the 110-150 ppm range, were indexed as shown in Figure 2(b).

Synthesis of boronated polybenzimidazole (B-PBI):

A three-necked flask was charged with 15 mL super anhydrous DMSO. To this flask 0.520 g (51 mmol, 1 eq.) of ABPBI was added. The flask was settled under vacuum for 1 h at 80°C to completely remove moisture. The temperature was then decreased gradually to room temperature. LiH (1.22 g) (153 mmol, 3 eq.) was transferred to another flask in a glove box under Ar atmosphere and was then dispersed in 8-10 mL of anhydrous DMSO. This dispersion was transferred by a syringe to the flask containing the ABPBI solution at room temperature while maintaining the anhydrous condition. The resulting mixture was stirred at room temperature for 24 h (the first step in Figure 1(a)). The reaction mixture was then stirred at 80 °C for another 1 h, after which it turned red indicating the formation of N-Li linkage due to its reaction with ABPBI. The reaction mixture was then cooled to ambient and 44 mL (94 mmol, 6 eq.) of triethylborane (BEt$_3$) (1mol/L) was added slowly over the period of 30 min while stirring on the ice bath. A yellow precipitate appeared which was dissolved when the mixture was hated to 80 °C. The reaction mixture was stirred for 24 h at this temperature (the second step in Figure 1(a)). After cooling the crude brown product was precipitated over
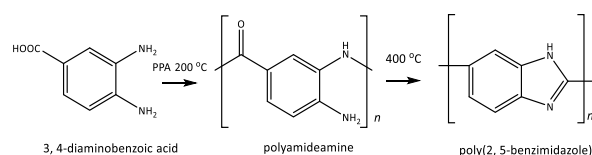
Scheme.1 Synthetic route of poly(2, 5-benzimidazole)
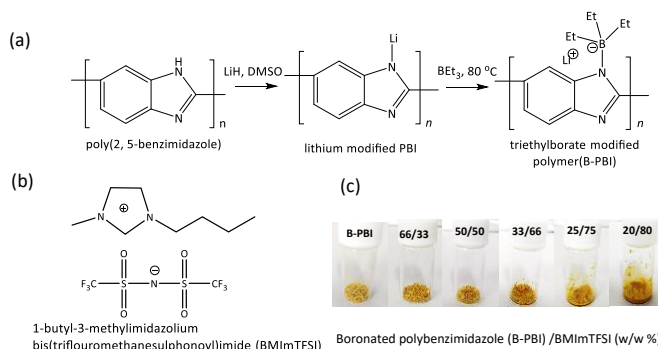
Fig. 1(a) Modification scheme of poly(2, 5-benzimidazole) to synthesize boronated polybenzimidazole, (b) Structure of the plasticizing agent for boronated polybenzimidazole, (c) Picture of the prepared composite polymer electrolyte

toluene-acetone (1:1) repeatedly. The product was dried in a vacuum oven for three days at 80 °C to finally obtain boronated polybenzimidazole (B-PBI). The final product was weighed 0.80 g (yield 84%).

The FT-IR spectrum of B-PBI (Figure 3a) showed characteristic peak[44] corresponding to B-N bending at 875 cm^{-1} and B-N stretching peak was merged with aromatic C=C peak at 1350 cm^{-1}, C=N was observed at 1500 cm^{-1}. The broad –NH peak on the other hand disappeared as the imidazole proton was substituted by triethylborane. Furthermore, the ^{11}B-NMR spectrum (Figure 3b) of B-PBI showed a single sharp peak (Figure 3b) at 2.73 ppm[45], confirming the sole presence of the quaternary borate B-PBI and the removal of the residual starting material.

Preparation of the B-PBI/BMImTFSI composite polymer electrolyte:

The typical procedure for preparing the composite polymer electrolytes is as follows: 0.1 g (4x10^{-6} mol) of B-PBI was taken in five different bottles to which BMImTFSI was added in different volumes (35 µL (1.2x10^{-4} mol), 70 µL (2.3x10^{-4}mol), 140 µL (4.8x10^{-4}mol), 210 µL (7.1x10^{-4}mol), and 280 µL (9.5x10^{-4}mol)) to prepare electrolyte mixtures with various weight compositions (66/33, 50/50, 33/66, 25/75, 20/80, respectively) [Figure 1(b)][31]. The electrolytes were sonicated at 40°C for 30 min to prepare homogeneous composite polymer electrolytes. The physical state of the prepared electrolytes changed from powder to paste like gel with an increase in the BMImTFSI amount as shown in Figure 1(c).

Materials and method:

3, 4-diaminobenzoic acid (3, 4-DABA) and poly(phosphoric acid) were used for the polymerization and were purchased from Tokyo Chemical Industries (TCI, Tokyo, Japan). Potassium hydroxide (KOH) and hydrochloric acid (HCl, 12M) were purchased from Kanto chemicals Co. Ltd. (Tokyo, Japan) were used for polymer synthesis. Methanol, acetone, hexane, diethyl ether, ethyl acetate and dimethylsulfoxide (DMSO) were purchased from Kanto chemicals Co. Ltd. were used as solvents without purification after received. Lithium hydride (LiH) was purchased from Sigma-Aldrich and triethylborate was purchased from Tokyo Chemical Industries (TCI, Tokyo, Japan) to prepare boronated polybenzimidazole. 1-Butyl-3-methylimidazolium Bis(trifluoromethanesulfonyl)imide was purchased from Tokyo Chemical Industries (TCI, Tokyo, Japan) and used as received. Ethylene carbonate: diethylene carbonate (EC: DEC) was purchased from Osaka Kishida chemical Co. Ltd. for battery fabrication.

The ^{11}B NMR spectra were recorded on a Bruker NMR spectrometer model AVANCE III 400 with BBFO plus ATMA probe operating at
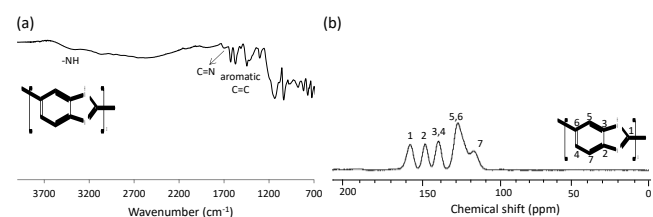
400.13 MHz and DMSO-d_6 was used as the NMR solvent. The ^{13}C solid-state NMR (cross polarization total sideband suppression/CPTOSS) spectra were recorded at 500 MHz on a Bruker Avance III spectrometer at a spinning speed of 8 kHz, using a standard cross-polarization pulse sequence. The samples were packed in a 7 mm-diameter zirconia rotor with a Kel-F cap and were spun at 10 kHz. A contact time of 2 ms was used and the period between the successive accumulations was 5 s. The number of scans was 10000. The FT-IR spectra of the polymers were recorded on a PerkinElmer Spectrum One spectrometer using a diamond-attenuated total reflection (ATR) mode. Thermo-gravimetric analysis (TGA) was conducted using a Hitachi STA7200. The samples (< 5 mg) were placed in a platinum crucible and were heated to a maximum temperature of 800 °C at a heating rate of 5 °C/min. The samples were tested under nitrogen atmosphere. The 5% (T_{d5}) and 10% (T_{d10}) degradation temperatures of the samples were also investigated along with their temperatures at the onset of degradation (T_{onset}). The ionic conductivity measurement has been done using a complex-impedance gain-phase analyzer (Solartron model 1260; Schlumberger, Germany) over the frequency range of 0.1 Hz–1 MHz. Lithium ion transference number of the samples was measured by the method described by Evans *et al*[32]. The measurements were carried out under an Ar atmosphere using identical Li electrodes and a potentiostat coupled with a frequency response analyser (Versastat-3; Princeton Applied Research Co. Ltd.). The impedance measurements were carried out over the frequency range of 100 kHz–10 mHz. A DC potential of 0.03 V (vs. Li/Li$^+$) was used during the polarization studies. Evans-Vincent-Bruce equation was used to calculate the t_{Li+} of the samples:

$$t_{Li+} = [I_s\,(\Delta V - I_oR_o)] / [I_o\,(\Delta V - I_sR_s)],$$

where I_0 and I_s are the initial and steady state current respectively, R_0 and R_s refer to the charge transfer resistance for the initial and steady states, respectively, ΔV is the DC potential applied across the cell and current determined by the DC polarization. Linear sweep voltammetry (LSV) measurements were performed in a sandwich cell with a Li/binary mixture electrolyte/Pt configuration. The measurements were performed at a scan rate of 10 mV/s, over the potential range of 0–6 V vs. Li/Li$^+$ using a BioLogic VSP s/n 1190 set-up. The charge-discharge analytical studies were carried out using a silicon-based anodic half-cell was prepared having CR2025 type coin cells with silicon as the working electrode (ϕ15 mm, Kindly donated by NISSAN Co.), lithium metal as the counter electrode (ϕ15 mm, Honjo metals, Japan) and a disc-shaped polypropylene based membrane (Celgard) as the separator (16 mm). The prepared silicon-based anodic half-cell was charged and discharged in a galvanostatic mode with a cut off potentials limit (1.5 V-0.01 V) at various current rate ranging between 0.1-2 C using compact charge and discharge system (EC Frontier; ECAD-1000). DEIS measurements were carried out on a VSP potentiostat (BioLogic)

Fig. 2 Spectra of poly (2, 5-benzimidazole) (a) FT-IR spectrum, (b) ^{13}C solid-state spectrum (cross polarization total sideband suppression) (CPTOSS)
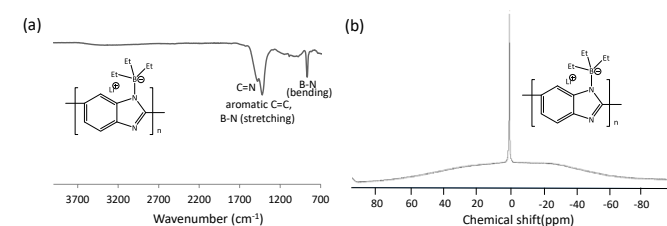
Fig. 3 Spectra of boronated polybenzimidazole (B-PBI) (a) FT-IR spectrum, (b) ^{11}B-NMR showing single borate peak

electrochemical analyser/workstation over a frequency range of 100 kHz-10 mHz with a sinus amplitude of 10 mV. The DEIS measurements were carried out at the open circuit potentials (OCP) of 1.650 V–0.01 V during charging and in the reverse direction during discharging. The step potential divided equally into 16 steps. Rheological measurements were carried out using a rheometer (MCR301, Anton Paar) with a stainless steel cone plate having a diameter of 25 mm (CP25, Anton Paar). The minimum torque which could be detected by the rheometer was 0.1 μN m. During the viscoelastic measurements, the temperature was maintained at 25.0 ± 0.1 °C using a Peltier plate. The samples were directly loaded in a nitrogen atmosphere. At first, a strain sweep test was carried out to determine the linear viscoelastic (LVE) region from the initial strain value of 0.01 to the final strain value of 10 with a constant frequency of 1 rad/s. The frequency sweep test was carried out in the LVE region (γ = 0.01%) over the frequency range of 0.01–60 rad/s.

Results and Discussion:

Physical characteristics:

Mechanical stability and degree of crystallinity of ABPBI:

The tensile stress–strain curve of the ABPBI film is shown in Figure S3. The curve showed a nonlinear region starting at about 65 MPa. The tensile strength of ABPBI was found to be 75 MPa and the Young's modulus, as calculated from the initial inclination of this curve, was 3.6 GPa, indicating that the film was strong and hard [47]. The crystalline structure of ABPBI was investigated by X-ray diffraction (XRD), which showed peak at a diffraction angle of 2θ= 26° (Figure S2)[48]. The degree of crystallinity of ABPBI was calculated using the method reported by Nara and Komiya et al [33]. To minimize the calculation error, baseline was drawn by using Origin pro software and the peak was decomposed into the crystalline portion and the amorphous area between 2θ of 10° and 50°. Degree of crystallinity in case of ABPBI was calculated to be 27 %, much higher than those of other amorphous polymers reported [34-35].

Thermal stabilities:

Figure S1 shows the TGA curves of ABPBI. The 5% (T_{d5}) and 10% (T_{d10}) weight loss temperatures of ABPBI in a N_2 atmosphere were as high as 600 and 700 °C, respectively, while those in an air atmosphere were 525 and 535 °C, respectively. These values are higher as compared with literature, where primary weight loss occurs around 200 °C due to water or solvent loss [46]. In our case we have preheated our pre-polymer samples at 350 °C for complete ring-closure and solvent removal. Figure 4 show the thermal weight loss curves of the electrolyte composites. The onset degradation temperatures of the composites were found to be within the range of 250–300 °C. The 5% (T_{d5}) and 10% (T_{d10}) decomposition temperatures of these composites are given in Table. 1. These temperatures were high enough for solid-state Li-ion battery applications. From the viewpoint of safety, thermally stable polymer electrolytes are in great demand for Li-ion batteries. In electric vehicles, the local temperature of batteries may approach 120 °C, which is near or higher than the boiling point of commercial liquid electrolytes. All the composite electrolytes maintain their residual weight in between 15-31 % of their primary weight even at

800 °C except B-PBI/BMImTFSI (w/w %) (20/80), it shows only 2 % residual mass at 800 °C. With increasing amount of added BMImTFSI, residual mass decreases except in the case of (25/75), which shows highest residual mass i.e. 31 %.

Rheological analysis:

Rheological study was made in order to confirm the solidity of B-PBI composites with BMImTFSI. Dynamic shear strain sweep test is
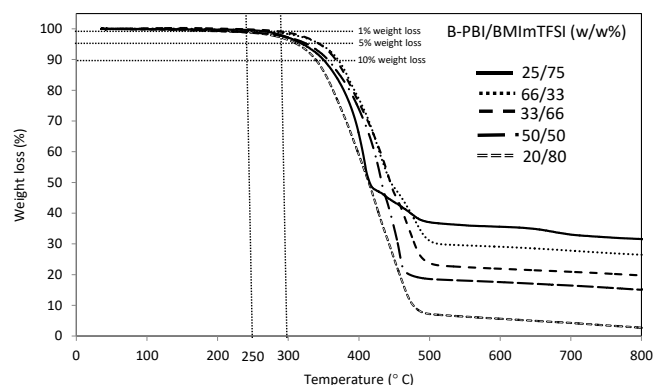
Fig. 4 Thermo-gravimetric analysis curves of the composite polymer electrolytes

Table.1 Thermal decomposition temperatures of boronated polybenzimidazole mixture with IL [a]

B-PBI/BMImTFSI (W/W%)	B-PBI(mol%)[b]	BMImTFSI(mol%) [c]	T_{d5}[d](°C)	T_{d10}[e] (°C)
66/33	100 mg (4x10⁻⁶)	35 μL (1.2x10⁻⁴)	340	375
50/50	100 mg (4x10⁻⁶)	70 μL (2.3x10⁻⁴)	345	370
33/66	100 mg (4x10⁻⁶)	140 μL (4.8x10⁻⁴)	335	368
25/75	100 mg (4x10⁻⁶)	210 μL (7.1x10⁻⁴)	325	355
20/80	100 mg (4x10⁻⁶)	280 μL (9.5x10⁻⁴)	310	340

(a) Thermal decomposition temperatures were determined by thermo-gravimetric analysis under N_2, (b) B-PBI: boronated polybenzimidazole; (c) BMImTFSI: 1-Butyl-3-methylimidazolium bis(trifluoromethanesulfonyl)imide which is used as the plasticizing agent ; (d) T_{d5} : 5% weight loss temperature measured by thermo-gravimetric analysis ; (e) T_{d10} : 10% weight loss temperature measured by thermo-gravimetric analysis

important to determine the viscoelastic region[36-37]. The dependence of storage and loss moduli (G', G'') on the shear strain (γ) and angular frequency (ω) B-PBI/BMImTFSI (25/75) (w/w %) is presented in Figure S4 (a, b). A linear region (Newtonian plateau) was observed at lower shear strains, while higher strains resulted in the formation of nonlinear regions. However, the G' values of the composites were higher than their G'' values even at the shear strains of >10%, indicating that the composites were predominantly solid. When a shear strain of 0.01% was used, the G' values were higher than the G'' values over the ω range of 0–100 (1/s). These results demonstrate the solidity of the 25/75 B-PBI/BMImTFSI (w/ w %) composites. Clearly, with lesser amount of added BMImTFSI, other electrolytes like B-PBI/BMImTFSI (w/w %) (66/33), (50/50) and (33/66) shows better solidity. On the other hand, in case of (20/80) solidity decreases further but keeps enough high value to use as composite solid electrolyte.

Electrochemical characterization:

Ionic conductivity measurements:

Ionic conductivities of the 66/33, 50/50, 33/66, 25/75 and 20/80 B-PBI/BMImTFSI (w/w %) composites were measured using the AC impedance method at several temperatures. Since these composite

electrolytes already contained lithium salts in the form of lithium borate in the side chain of B-PBI, the addition of any lithium source was not required unlike in the case of most of the commercial polymer electrolytes[38-41]. Prior to the measurements, the samples were dried thoroughly for 24 h at 100 °C under vacuum. The ionic conductivity of the samples increased constantly with temperature (Figure 5a). At 51 °C, the composite electrolytes showed an ionic conductivity in the range of 3.0–8.8x10^{-3} S cm^{-1} (Table 2). The ionic conductivity of the electrolytes increased with an increase in their IL content. The 25/75 electrolyte showed the highest ionic conductivity of 8.8x10^{-3} S cm^{-1} at 51 °C. The ionic conductivities of the electrolytes developed in this study were at least 10 times higher than those of the electrolytes reported previously, which required externally added lithium salts (Table 2). The 66/33 electrolyte had the highest B-PBI content was mainly solid in nature. The liquid nature of the electrolytes was induced by the addition of BMImTFSI. As the BMImTFSI content increased, the number of carrier ions increased, which can be explained as migration of Li$^+$ cation increases due to plasticizing behaviour of ionic liquid. The Arrhenius plots of the electrolytes showed linear profiles with an increase in temperature, indicating that no decomposition or phase change occurred over the measured temperature range (Figure 5a). The Vogel-Fulcher-Tammann[42] (VFT) plots (Figure 5b) of the electrolytes were fitted according to the linear regression equation and the parameters so obtained are listed in Table

$$\sigma_{(t)} = A / \sqrt{T} \ \exp[-B / (T - To)]$$

In the above equation $\sigma_{(t)}$ is the ionic conductivity at temperature T, whereas T_0 is the ideal glass transition temperature which was optimized to obtain linear VFT plot. 'A' and 'B' refer to the number
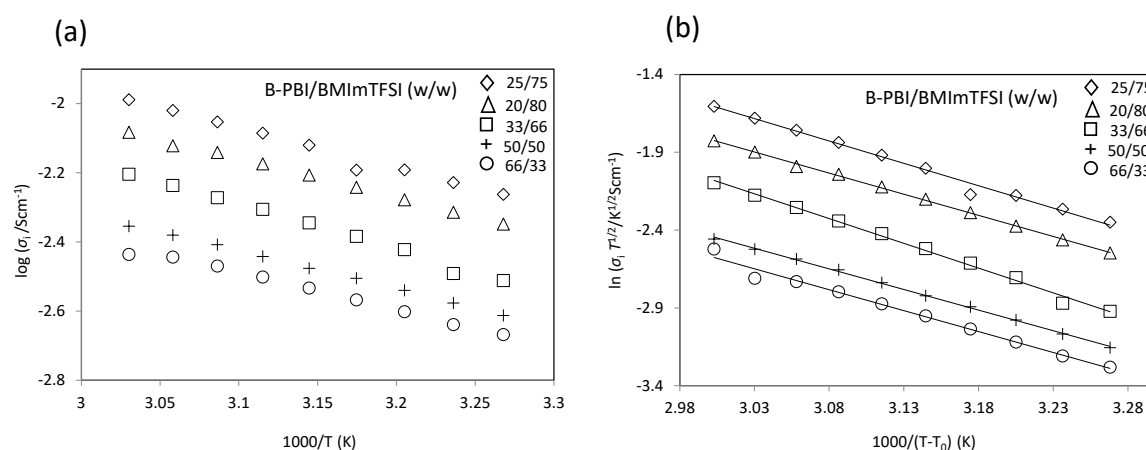
Fig. 5 Ionic conductivity measurements of various composites between boronated polybenzimidaozole with BMImTFSi (a) Arrhenius plots and (b) Vogel-Fulcher-Tammann(VFT) plots

Table.2 VFT parameters, lithium transference number (t_{Li}^+) and working potential window of various composite polymer electrolytes

B-PBI: BMImTFSI	Ionic conductivity (Scm^{-1}) at 51°C[a]	Carrier ion number, A (K$^{1/2}$Scm^{-1}) [b]	Activation energy, B (K) [c]	R^2 [d]	Lithium Transference number at r.t.[e]	Li-ion conductivity (Scm^{-1}) [f]	Working potential window(V)[g]
66/33	3.4X10^{-3}	158.7	2850.2	0.997	0.27	9.2X10^{-4}	ND
50/50	3.9X10^{-3}	239.2	2666.3	0.998	0.42	1.6X10^{-3}	4.85
33/66	5.3X10^{-3}	1127.9	2545.7	0.999	0.51	2.7X10^{-3}	5.45
25/75	8.8X10^{-3}	1356.1	2433.2	0.999	0.63	5.5X10^{-3}	5.22
20/80	7.2X10^{-3}	1297.3	2531.6	0.999	0.57	4.1X10^{-3}	ND
[41](PEO)$_8$LiClO$_4$	2.4X10^{-4} (at 70°C)	-	-	-	0.20	4.8X10^{-5}	4.2
[39]PEG-borate ester LiClO$_4$	1.0X10^{-3} (at 70°C)	-	-	-	0.24	2.4X10^{-4}	4.2
[40]PVDF-HFP/LiClO$_4$	1.06X10^{-3} (at r.t.)	-	-	-	0.36	3.8X10^{-4}	4.5
[38]Nafion (Li$^+$)	2.05X10^{-4} (at r.t.)	-	-	-	0.89	1.8X10^{-4}	4.2

(a) Temperature varying ionic conductivity measured by using AC impedance method, (b) Carrier ion number resemblance total number of charge carrier ions, (c) activation energy must be lower to make ion conduction easier, (d) R²: Regression co-efficient, (e) Li- transference number was determined by using DC polarization and AC impedance method, (f) ionic conductivity contributed by cationic (Li⁺-ion) conduction, (g) Determined using linear sweep voltammetry technique

of carrier ions and activation energy for ion transport respectively. With an increase in the BMImTFSI amount, the number of carrier ions increased, while the activation energy decreased. Chronoamperometry experiments were performed to check the Li-ion diffusion in the composite electrolyte matrix. Steady-state current profiles obtained in the DC polarization method (Figure S5) of the Li/electrolyte/Li-type cells, implies that Li ions were successfully incorporated into the polymer during modification[43].

Lithium transference number:

The contribution of lithium cation migration under the ionic conduction of various ionic species was denoted by t_{Li^+}. It was estimated using the method reported by Evans et al., which combined the DC polarization and AC impedance techniques[32]. All the measurements were carried out by chronoamperometry and impedance analysis, and the error margin was less than ± 1%. The highest t_{Li^+} was observed to be 0.63 at room temperature for (25/75) B-PBI/BMImTFSI (w/w %) among the entire composite polymer electrolytes (Table 2) while lithium ion conductivity of the same is in the order of 10^{-3} Scm^{-1}. With an increase in the IL content, the t_{Li^+} of the polymer ion gels increased monotonously till it reached the value of 0.63 for the (25/75) B- PBI/BMImTFSI (w/w %) composite electrolyte. This was unexpected observation; however, it can be attributed to the fact the efficient plasticization of solid polymer-salt hybrid electrolytes makes them highly dissociable. The lithium transference numbers of the composite electrolytes developed in this study and those reported previously are compared in Table 2, which clearly demonstrates the superior characteristics of the electrolytes developed in this study.

Plausible mechanism responsible for high ionic conductivity:

Polybenzimidazole (PBI) itself is basically a non-conjugated polymer. However, the imidazolate anion formed after the lithiation and boronation of its imidazole moiety, has six π-electrons, which induce aromaticity. Therefore B-PBI with lithiated and boronated imidazole moiety can be regarded as a unique type of π-conjugated polymer (Scheme 2). In the case of the electrolytes developed in this study, anionic charge was delocalized on the PBI-derived conjugated polymer, which reduced the site hopping energy of lithium ions. This specific situation will be responsible for markedly high ionic conductivity and lithium transference number of the resulting polymer ion gel electrolyte. This phenomenon is conceptually novel. Boron atom also receives a considerable number of electrons; however, the boronation of imidazole unit should not be quantitative. In spite of the efficient delocalization of
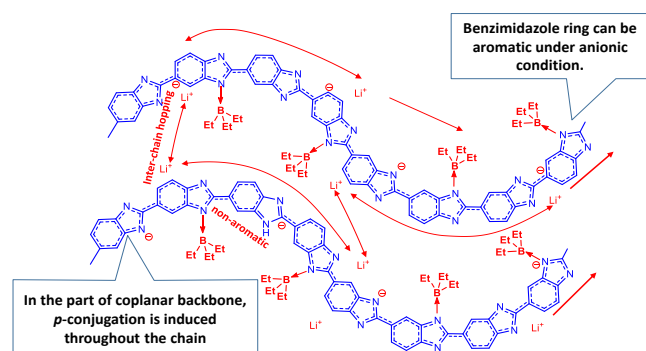
anionic charge, long range electronic conduction occurs along the conjugated chains, which can prevent lithium ion transport. However non-quantitative boronation breaks the π-conjugation to inhibit the electronic conduction, thus increasing the high lithium transference number significantly.

Linear sweep voltammetry measurements:

Apart from the thermal stability of the electrolytes, their electrochemical stability, which is another important factor for their application in high-potential batteries, was also evaluated by linear sweep voltammetry (LSV) measurements. The LSV measurements were carried out using the Li/electrolyte/Pt cell configuration at a scan rate of 10 mVs^{-1} over the potential range of 0–6 V. The 50/50, 33/66, and 25/75 B-PBI/BMImTFSI (w/ w %) electrolytes showed an electrochemical potential window of 4.85–5.45 V. It can be seen from the linear sweep voltammograms (Figure 6) that after a certain voltage in each case there was a sudden increase in the current, indicating the occurrence of electrochemical degradation. However, the potential window range in this study was wider than that reported for other polymer electrolytes (Table 2). Hence, the electrolytes developed in this study are suitable for high-potential Li-ion batteries.
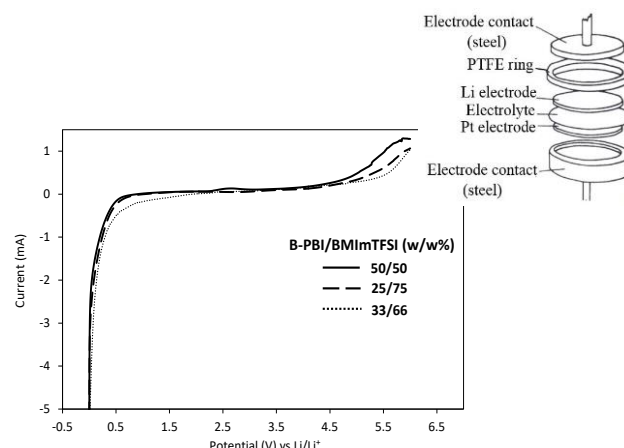
Fig.6 Linear sweep voltammetry curves of various composites of boronated polybenzimidaozle and BMImTFSI

Inset: Cell set-up for linear sweep voltammetry measurements

Battery performance:

Because of its high ionic conductivity and t_{Li^+}, (25/75) B-PBI/BMImTFSI (w/w %) was further subjected to electrochemical studies. Charge-discharge characteristics were studied for the composition B-PBI/BMImTFSI 25/75 (w/w %) in a coin type anodic half-cell. The CR2025coin-type anodic half-cell consisted of silicon as the working electrode, Li metal as the counter electrode, a polypropylene separator, and the composite polymer as the electrolyte (ca. 30 mg). Ethylene carbonate: diethylene carbonate (EC: DEC) solution (25-30 μL) was used to wet the electrode surface. The application of the EC: DEC accelerated the formation of the solid electrolyte interface (SEI) layer through the interaction with the electrode. The cell was assembled in a glove box under an argon atmosphere (UNICO UN-650F, H_2O and O_2 content <0.1 ppm). The assembled cell was kept undisturbed overnight for stabilization. First, the anodic half-cell was subjected to two cycles at 0.05 C rate. Highly irreversible capacity was observed during these cycles because of the formation of the SEI layer.

Scheme 2: Speculated mechanism of lithium ion conduction in the system
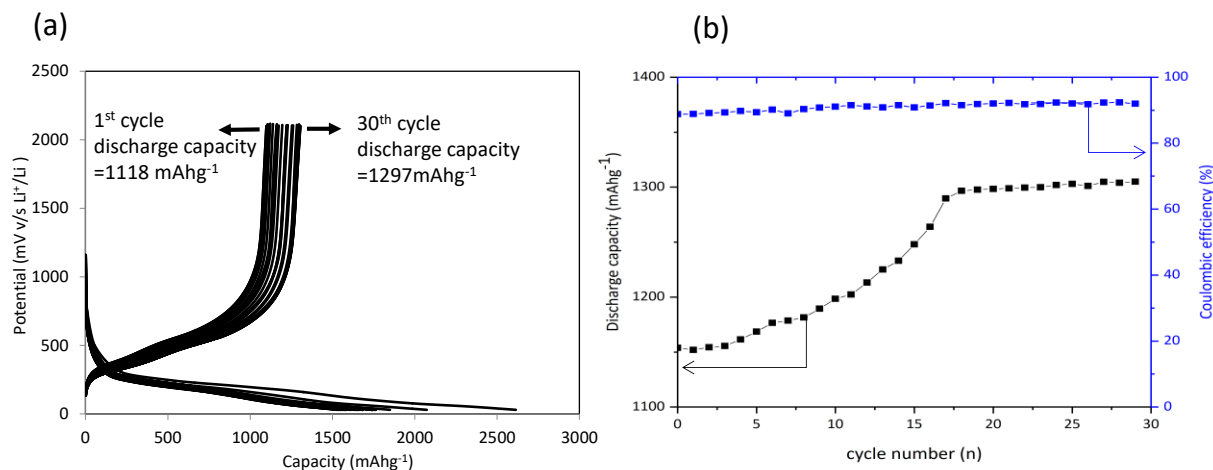
Fig. 7 Charge-discharge measurements of the Li/electrolyte/Si cell fabricated using (25/75) B-PBI/BMImTFSI (w/w %) polymer electrolyte at 0.1C (a) Charge-discharge profile (b) Discharge capacity and Coulombic efficiency
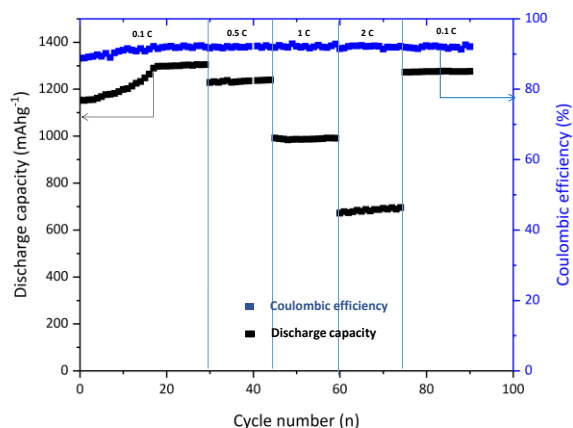
Fig. 8 Rate cycling performance of the Li/electrolyte/Si cell fabricated using the (25/75) B-PBI/BMImTFSI (w/ w%) polymer electrolyte for 65 cycles at various rates (cycle 0-19 at 0.1 C, 20-34 at 0.5 C, 35-49 at 1 C and 50-64 at 2 C)

It was then subjected to 30 more cycles at 0.1 C rate, the result of charge-discharge is shown in Figure 7(a). Figure 7(b) shows the cycling performance (the discharge capacity and Coulombic efficiency) of the composite electrolyte at 0.1 C rate. The discharge capacity increased with an increase in the number of cycles, indicating that a stable conductive SEI layer was formed during this period. After 18 cycles of increasing values, discharge capacity got stabilized for the next 12 cycles at the same charging rate. The Coulombic efficiency of the electrolyte increased with an increase in the number of cycles because of the formation of a good SEI layer. Figure 8 shows the cycling performance of the cell at variable charging rates of 0.1 C–2 C. The discharge capacity and Coulombic efficiency values were plotted as a function of the number of cycles. When the current rate was increased by five times i.e., from 0.1 C to 0.5 C (30th–44th cycle), discharge capacity decreased as expected. However, the discharge capacity stabilized with an increase in the number of cycles at 0.5 C. At the current rate of 1C (45th–59th cycle), discharge capacity decreased, while the Coulombic efficiency showed constant values. When the current rate was further increased to 2 C (60th–74th cycle), the discharge capacity decreased further, whereas the Coulombic efficiency remained constant for almost all the current rates. Most importantly when it reverts to lower charging rate of 0.1 C (75th–89th cycle), the cell produced
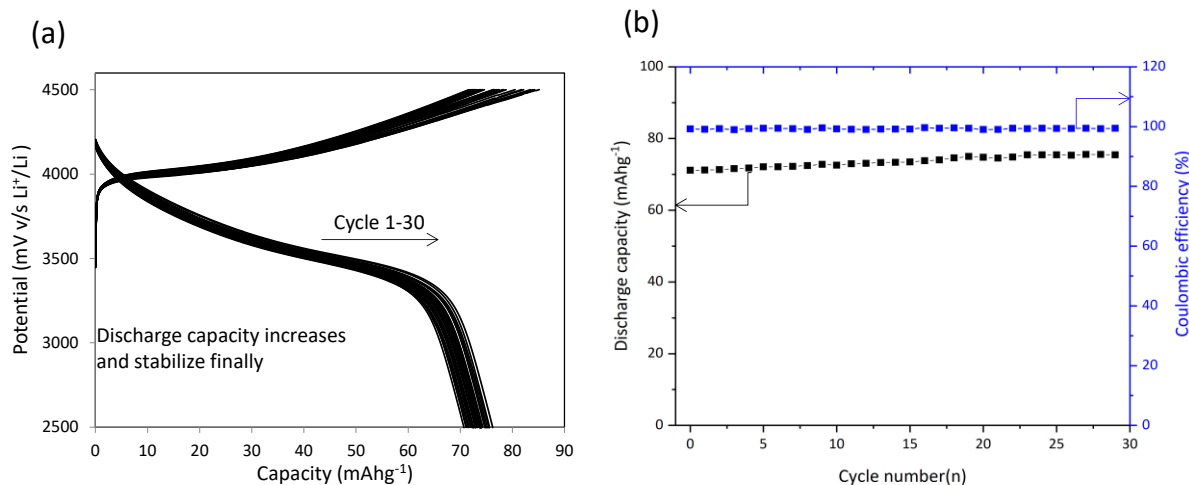
Fig. 9 Charge-discharge measurements of the Li-MNC/electrolyte/Li cell fabricated using (25/75) B-PBI/BMImTFSI (w/w %) polymer electrolyte at 0.1C (a) Charge-discharge profile (b) Discharge capacity and Coulombic efficiency

Please do not adjust margins

discharge capacity around 1275 mAhg⁻¹ with constant coulombic efficiency, exhibiting the structural stability of the cell. These results indicate that the formation of the SEI layer occurred via a reaction between the EC: DEC solvent and the electrode. The SEI layer stabilized with time at both the lower and higher rates. Furthermore, cathodic half-cell was also prepared using $LiNi_{0.33}Co_{0.33}Mn_{0.33}O_2$ (Li-MNC)/electrolyte/Li cell to perform charge-discharge at high potential (~4.5 V). Similar to the anodic half-cells, we have performed charge-discharge for 30 cycles at 0.1 C as shown in figure 9(a, b). Stable SEI layer formation was depicted from increasing trend of discharge capacity even at higher potential range, which in the other way exhibits electrochemical stability of the prepared electrolyte.

Dynamic electrochemical impedance spectroscopy measurements:

In the classic EIS method, impedance measurements are carried out after the battery reaches a steady state, for which there is no direct current. Hence, during the equilibrium state of the battery experiencing zero DC potential, the real picture of the interfacial process cannot be depicted using EIS. Recently, DEIS has been introduced as characterization technique to determine the electrochemical responses of interfacial phenomenon. This technique provides variable frequency response of an AC signal superimposed with a potentiodynamic DC voltage during potential scan of anodic half-cells. This technique offers various advantages over the conventional EIS method such as: real time information can be observed during charging or discharging and the formation of the SEI layer can be examined in detail[20-21]. The anodic half-cell was fabricated using the 25/75 B-PBI/BMImTFSI (w/ w %) polymer electrolyte. The DEIS measurements (measuring the impedance during charging and discharging at various potentials) were performed after overnight stabilisations. During the first 20 cycles (Figure 8) the reversible capacity increased and stabilized with an increase in the number of cycles at the current rate of 0.1 C. At 0.5 C rate, a stable reversible capacity was observed for 15 cycles. This trend continued for higher current rates. This can be attributed to the formation of the SEI layer and lithium intercalation, as discussed in the previous section. To investigate the effect of cycling on the formation of the SEI layer in detail, the same cell was cycled at the rate of 0.5 C for 10 cycles, followed by the charge-discharge DEIS measurement in the similar fashion. Figures 10(a, b) show the DEIS profiles of the anodic half-cell during charging and discharging, respectively. These figures compare the variation in the R_{SEI} (Li⁺ transport resistance through the SEI layer) with respect to the potential for both the cases of freshly prepared and already pre-cycled anodic half-cell. Close look at Figure 10 (a and b) i.e. comparing between the DEIS charging profiles before and after

(a)

(b)
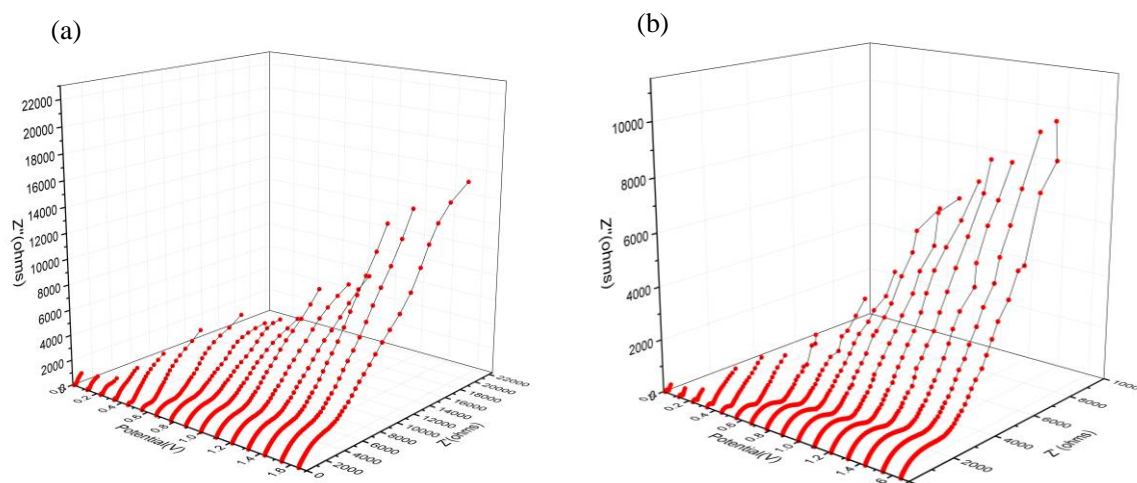
Fig. 10 DEIS profile of the (a) freshly prepared and (b) pre-cycled (10 cycles) anodic half-cells fabricated using the (25/75) B-PBI/BMImTFSI (w/ w %) polymer electrolyte at the charging rate of 0.5 C

(a)

(b)
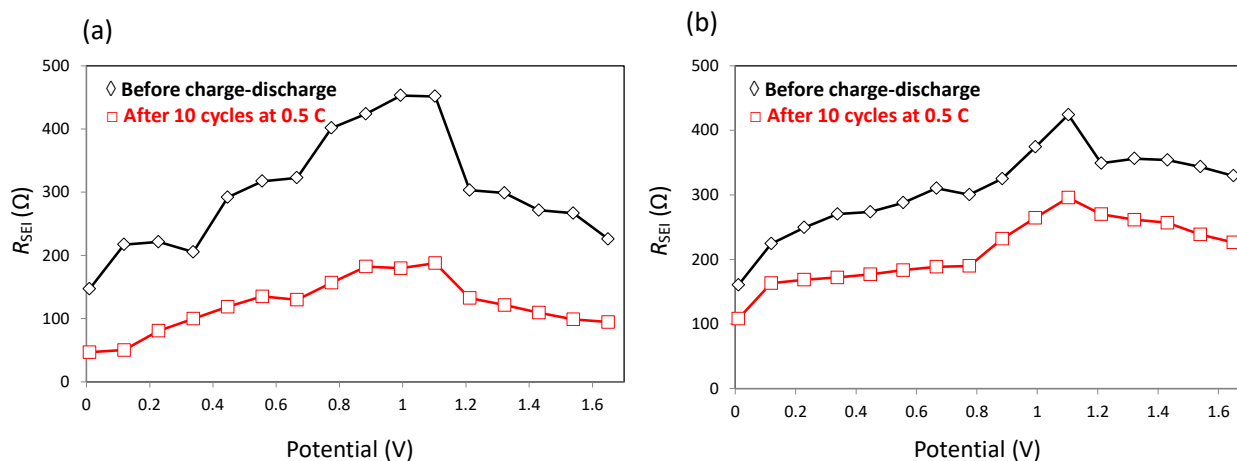
Fig. 11 R_{SEI} of the pre-cycled and freshly prepared anodic half-cell fabricated using the (25/75) B-PBI/BMImTFSI (w/ w %) polymer electrolyte as a function of the potential (a) during charging and (b) discharging

cycling it is clearly observed that semicircle radii i.e. R_{SEI} at higher frequency were restrained in case of pre-cycled cell as compared with that of the freshly prepared cell. Similar observations were found for the DEIS discharging profiles as well [Figure S6 (a, b)] i.e. overall radii of the semicircles are getting diminished in case of pre-cycled cell as compared with the freshly prepared cell.

For the quantitative analysis, impedance data was fitted to the equivalent electric circuit models (EECMs) from the corresponding Nyquist and Bode plots[32]. The R_{SEI} impedance values of both the pre-cycled and freshly prepared cells during the charging and discharging process obtained from the DEIS measurements were plotted against the potential (Figures 11(a, b)). The circuit fitting results also supported the formation of a stable interface, which resulted in a decrease in the R_{SEI}, thus improving the reversible capacity of the pre-cycled cell.

Conclusion:

Poly (2, 5-benzimidazole) (ABPBI) was modified by the formation of lithium imidazolate formation by complex formation with triethylborane to design ionic B-PBI. Further, it was mixed with BMImTFSI to prepare various composite polymer electrolytes (B-PBI/BMImTFSI (w/w %)) exhibiting high ion conductivity. All these composites showed thermal stability at temperatures in the range of 250–300 °C and an average 10% weight loss temperature (T_{d10}) as high as 350 °C. The solidity of the composites was evaluated by rheological measurements, which revealed that their storage modulus was higher than the loss modulus. Ionic conductivity and Li-ion transference number t_{Li}^+ were measured for the composite series and better properties were observed as BMImTFSI content increase relative to B-PBI. The (25/75) B-PBI/BMImTFSI (w/ w %) composite showed the highest ionic conductivity and t_{Li}^+ of 8.8×10^{-3} S cm^{-1} and 0.63, respectively. The LSV measurements revealed that the composites showed a wide potential window of 4.85–5.45 V, which is high enough for high-energy battery applications. Battery performance was evaluated using the (25/75) B-PBI/BMImTFSI (w/ w %) composite and discharge capacity showed stable profiles at different charge-discharge rates and even at a high current rate of 2 C more than 53% of reversible capacity remains as compared with the rate of 0.1 C. The composite showed a Coulombic efficiency of >90% irrespective of the current rate. Furthermore, Li-MNC cathodic half-cell were also fabricated to check high voltage charge-discharge cycling, which also exhibits electrochemical stability of the electrolyte. DEIS study was carried out as a novel technique to investigate the interfacial properties of the composite electrolyte-based anodic half-cell before and after charge-discharge cycling. The R_{SEI} of the cell decreased after cycling, indicating that cycling resulted in the formation of a stable SEI layer.

Conflicts of interest

There are no conflicts of interest to declare

Acknowledgements

Notes and references

1. P. G. Bruce, B. Scrosati, J-M. Tarascon, *Angew. Chem. Int. Ed.*, 2008, **47**, 2930 – 2946.
2. J. M. Tarascon, M. Armand, *Nature*, 2001, **414**, 359-367.
3. E. Quartarone, P. Mustarelli, *Chem. Soc. Rev.*, 2011, **40**, 2525-2540.
4. K. Deng, S. Wang, S. Ren, D. Han, M. Xiao, Y. Meng, *ACS Appl. Mater. Interfaces*, 2016, **8**, 33642–33648.
5. L. Porcarelli, A. S. Shaplov, M. Salsamendi, J. R. Nair, Y. S. Vyogdskii, D. Mecerreyes, C. Gerbaldi, *ACS Appl. Mater. Interfaces*, 2016, 8, 10350-10359.
6. Y. Zhang, J. Lai, Y. Gong, Y. Hu, J. Liu, C. Sun, Z. L. Wang, *ACS Appl. Mater. Interfaces*, 2016, **8**, 34309-34316.
7. H. Hou, Q. Xu, Y. Pang, L. Li, J. Wang, C. Zhang, C. Sun, Adv. Sci., 2017, **4**, 1700072.
8. M. Wakihara, *Mater. Sci. Eng.*, 2001, **R33**, 109-134.
9. N. Matsumi, M. Nakashiba, T. Mizumo, H. Ohno, *Macromolecules,* 2005, **38**, 2040-2042.
10. H. Zhang, C. Li, M. Piszcz, E. Coya, T. Rojo, L. M. Rodriguez-Martinez, M. Armand, Z. Zhou, *Chem. Soc. Rev.*, 2017, **46**, 797-815.
11. N. Matsumi, K. Sugai, H. Ohno, *Macromolecules*, 2002, 35, 5731-5733.
12. Matsumi, N., Mizumo, T., Ohno, H. *Chem. Lett.,* 2004, **33(4)**, 372-373.
13. B. Qin, Z. Liu, J. Zheng, P. Hu, G. Ding, C. Zhang, J. Zhao, D. Kong, G. Cui, *J. Mater. Chem. A*, 2015, **3**, 7773-7779.
14. H. Gupta, Shalu, L. Balo, V. K. Singh, S. K. Singh, A. K. Tripathi, Y. L. Verma, Singh, R. K. *Solid State Ionics*, 2017, 309, 192-199.
15. G. A. Tiruye, D. Munoz-Torrero, J. Palma, M. Anderson, R. Mercilla, *J. Power Sources*, 2015, **279**, 472-480.
16. K. S. Liao, T. Sutto, E. Andreoli, P. Ajayan, K. A. McGrady, S. A. Curran, *J. Power Sources*, 2010, **195**, 867–871.
17. H. Ye, J. Huang, J. J. Xu, A. Khalfan, S. G. Greenbaum, *J. Electrochem. Soc.*, 2007, **154(11)**, A1048-A1057.
18. C. Sun, J. Liu, Y. Gong, D. P. Wilkinson, J. Zhang, Nano Energy, 2017, **33**, 363-386.
19. Ye, Y-S., Rick, J., Hwang, B-**J.** *J. Mater. Chem. A**, 2013, **1**, 2719-2743.
20. Smaran, K. S., Joshi, P., Vedarajan, R., Matsumi, N. *ChemElectroChem*, 2015, **2(12)**, 1913-1916.
21. S. G. Patnaik, R. Vedarajan, N. Matsumi, *J. Mater. Chem. A*, 2017, **5(5)**, 17909-17919.
22. J. Huang, Z. Li, J. Zhang, *Journal of Power Sources*, 2015, **273**, 1098-1102.
23. Q. Ma, H. Zhang, C. Zhou, L. Zheng, P. Cheng, J. Nie, W. Feng, Y. S. Hu, H. Li, X. Huang, L. Chen, M. Armand, Z. Zhou, *Angew. Chem. Int. Ed.,* 2016, **55**, 2521-2525.
24. S. Feng, D. Shi, F. Liu, L. Zheng, J. Nie, W. Feng, X. Huang, M. Armand, Z. Zhou, *Electrochim. Acta*, 2013, **93**, 254-263.
25. F. Bertasi, G. Pagot, K. Vezzu, E. Negro, P. J. Sideris, S. G. Greenbaum, H. Ohno, B. Scrosati, V. D. Noto, J. Power Sources, 2018, **400**, 16-22.
26. R. S. Bhavsar, S. C. kumbharkar, A. S. Rewar, U. K. Kharul, *Polym. Chem.*, 2014, **5**, 4083-4096.

27. M. Jung, W. Lee, N. N. Krishnan, S. Kim, G. Gupta, L. Komsiyska, C. Harms, Y. Kown, D. Henkensmeier, *Appl. Surf. Sci.,* 2018, **450**, 301-311.

28. G. Nawn, G. Pace, S. Lavina, K. Vezzu, E. Negro, F. Bertasi, S. Polizzi, V. D. Notto, *Macromolecules*, 2015, **48**, 15-27.

29. G. Nawn, K. Vezzu, F. Bertasi, G. Pagot, G. Pace, F. Conti, E. Negro, V. D. Notto, *Electrochim. Acta*, 2017, **228**, 562-574.

30. J. Huang,Z. Li, B. Y. Liaw, J. Zhang, 2016, *Journal of Power Sources*, **309**, 82-98.

31. Shalu, V. K. Singh, R. K. Singh**,** *J. Mater. Chem. C*, 2015, **3**, 7305-7318.

32. J. Evans, C. A. Vincent, P. G. Bruce, *Polymer*, 1987, **28(13)**, 2324-2328.

33. S. Nara, T. Komiya, *Starch – Stärke*, 1983, **35(12)**, 407-410.

34. O. Martin, L. Averous, *Polymer*, 2001, **42**, 6209-6219.

35. V. E. Reinsch, L. Rebenfeld, *J. Appl. Polym. Sci.*, 1996, **59(12)**, 1913-1927.

36. T. Mitsumata, T. Miura, N. Takahashi, M. Kawai, M. K. Okajima, T. Kaneko, *Phys. Rev. E*, 2013, **87**, 042607.

37. J. L. Schaefer, S. S. Moganty, D. A. Yanga, L. A. Archer, *J. Mater. Chem. A*, 2011, **21**, 10094-10101.

38. M. Wang, F. Zhao, S. Dong, *J. Phys. Chem. B,* 2004, **108**, 1365-1370.

39. Y. Kato, S. Yokoyama, T. Yabe, H. Ikuta, Y. Uchimoto, M. Wakihara, *Electrochim. Acta*, 2004, **50**, 281-284.

40. W. Liu, X. K. Zhang, F. Wu, Y. Xiang, *IOP Conf. Ser.: Mater. Sci. Eng.,* 2017, **213** 012036.

41. H. Y. Sun, H. J. Sohn, O. Yamamoto, Y. Takeda, N. Imanishi, *J. Electrochem. Soc,* 1999, **146 (5),** 1672-1676.

42. A. Perez-Madrid, *J. Chem. Phys.*, 2005, **122**, 214914.

43. A. Singh, R. Vedarajan, N. Matsumi, *J. Electrochem. Soc.*, 2017, **164 (8),** H5169-H5174.

44. X. Luo, Y, Zhang, C. Zanden, M. Murugesan, Y. Cao, L. Ye, J. Liu, *J Mater Sci: Mater Electron,* 2014, **25**, 2333-2338.

45. R. A. Oliveira, R. O. Silva, G. A. Molander, P. H. Menezes, *Magn.Reson.Chem.*, 2009, **47,** 873–878.

46. J. W. Lee, K. Kim, S. B. Khan, P. Han, J. Seo, W. Jang, H. Han, *J. Nanomater.*, 2014, ID 460232, 1-7.

47. Q. Li, J. O. Jensen, R. F. Savinell, N. J. Bjerrum*, Prog. Polym. Sci.*, 2009, **14**, 449-477.

48. J. A. Asensio, S. Borros, P. G. Romero, *J. Electrochem. Soc.*, 2004, **151 (2),** A304-A310.